Progress In Electromagnetics Research, Vol. 128, 291–311, 2012

ADAPTIVE CLUTTER SUPPRESSION FOR AIRBORNE RANDOM PULSE REPETITION INTERVAL RADAR BASED ON COMPRESSED SENSING

Z. Liu*, X. Z. Wei, and X. Li

Research Institute of Space Electronics Information Technology, School of Electronic Science and Engineering, National University of Defense Technology, Changsha 410073, China

Abstract—We present an adaptive clutter suppression method for airborne random pulse repetition interval radar by using prior knowledge of clutter boundary in Doppler spectrum. In this method, by exploiting the intrinsic sparsity, compressed sensing based on iterative grid optimization (CS-IGO) is applied to directly recover the clutter spectrum with only the test range cell instead of nonhomogeneous training data from adjacent range cells. Since the sensing matrix and clutter spectrum obtained by CS-IGO are well adapted to the data, the prewhitening filter can be effectively obtained to cancel the mainlobe clutter. Further, the clutter residue can be suppressed by the iterative reweighted l_1 minimization to enhance the target response. Simulation results show that the approach is capable of effective suppression of clutter and precise recovery of targets' unambiguous spectrum, offering a high performance of output signal to clutter and noise ratio.

1. INTRODUCTION

Random selection of the pulse repetition intervals (PRI) within fixed coherent process interval (CPI) as a means of smearing the ambiguity peaks has been alluded to in the past [1–3], which can achieve great ECCM capabilities. Traditional processing approach for the random PRI radar signal such as correlation is constrained by the uncertainty principle and suffers from high sidelobe pedestal, which reduces the performance of target detection and velocity measurement. Considering of the random modulation scheme and the inherent

Received 20 February 2012, Accepted 21 May 2012, Scheduled 1 June 2012

* Corresponding author: Zhen Liu (zhen_liu@nudt.edu.cn).

sparsity of the target echo signal, the compressed sensing (CS) theory [4–8] has been applied to successfully resolve the velocity ambiguity and suppress the sidelobe pedestal [9].

In some actual applications such as airborne systems, however, echoes form land clutter consisting of stable objects like mountains and buildings [10] can violate the assumptions for CS severely [11], which needs to be investigated. By now, several literatures have directly addressed to alleviate strong clutter interference [9, 11–13], where the approaches can be classified into two groups. One is pre-filtering before CS recovery that is mathematically represented as a projection to the clutter free subspace [11, 12], and the other is weighting the clutter support combined with CS optimization [9, 13], which is actually a sparsity enhancing technology [14]. Both of the methods have a common point that the clutter spectrum needs to be estimated as a prior knowledge for clutter cancellation. Therefore, the key requirement is the accurate estimation of power spectral density (PSD) of clutter.

Traditionally, statistical spectrum estimation methods such as autoregressive model [9] need sufficient statistically independent and identically distributed (i.i.d.) training data to obtain an effective estimation of the clutter. However, if the clutter scenario is not homogeneous, the range stationarity is destroyed, which results in an inaccurate estimation of the clutter distribution [15]. Referring to the direct data domain (D3) approach designed for space-time adaptive processor (STAP) [15–17], we exploit the priori sparsity of the clutter spectrum and propose a new approach to obtain the high-resolution spectrum with only the test cell.

In this paper (which expands upon [18]), the recently developed CS algorithm based on iterative grid optimization (CS-IGO) with slight grid mismatch is applied to recover the Doppler spectrum. Since the sensing matrix and spectrum obtained by CS-IGO are well adapted to the data, there is almost no clutter sidelobe in the spectrum and then the clutter echo can be obtained by using prior knowledge of its boundary. This guarantees the availability of clutter covariance matrix (CCM) and corresponding adaptive prewhitening filter, which can effectively cancel the mainlobe clutter. Moreover, referring to the sparsity enhancing technology, the iterative reweighted l_1 minimization is introduced to suppress the clutter residue and boost the target response. Simulation results show that the approach offers a high performance of output signal to clutter and noise ratio (SCNR) in the nonhomogeneous clutter scenario.

The remainder of this paper is organized as follows. In the next section, we mainly introduce the echo signal model of random PRI

radar and exploit the sparsity of spectrum for estimation. Section 3 constructs the clutter suppression sketch by the pre-filter and iterative reweighted l_1 minimization. Section 4 makes some complementary discussions. In Section 5 simulations and numerical illustrations are used to test the performance of clutter estimation and suppression. Some analyses are given as well. Finally, the conclusions are drawn in the last section.

2. DATA MODEL AND SPECTRUM ESTIMATION WITH CS-IGO

2.1. Data Model

In random PRI radar we transmit M pulses at T_m, which is i.i.d. within the CPI $(0, MT_r)$ randomly where T_r is the average PRI. Then the transmitted signal can be represented as

$$s(t) = \sum_{m=0}^{M-1} A \operatorname{rect}\left(\frac{t - T/2 - T_m}{T}\right) \exp(j2\pi f_0 t) \tag{1}$$

where $\operatorname{rect}\left(\frac{t}{T}\right) = \begin{cases} 1, & -T/2 \le t \le T/2 \\ 0, & \text{else} \end{cases}$, $m = 0, 1, \ldots, M-1$, A is the pulse amplitude, f_0 the carrier frequency, and T the pulse width.

Suppose that there are K targets in the test range cell moving toward the radar with radial velocity v_k. The received signal is generated as the sum of the Doppler-shifted replicas of the transmitted waveform, each of which is multiplied by the respective scattering coefficient. Sampling the received signal of mth pulse after down-conversion and low-pass filtering can obtain

$$s_r[m] = \sum_{k=1}^{K} A_k \exp(j2\pi \upsilon_k T_m) \tag{2}$$

where A_k is the complex amplitude proportional to the square root of target radar cross section (RCS), and $\upsilon_k = 2f_0 v_k / c$ is the Doppler frequency of the k-th target. Obviously, (2) can be regarded as a typical underdetermined linear system

$$\mathbf{s}_r = \mathbf{\Theta}(\xi)\boldsymbol{\alpha} + \mathbf{w} \tag{3}$$

when we consider N ($> M$) Doppler 'grids' at $\xi[n]\delta_\upsilon$, where $\mathbf{s}_r = [s_r[0], s_r[1], \ldots, s_r[M-1]]^T$, $\xi = [\xi[0], \xi[1], \ldots, \xi[N-1]]^T$, $\mathbf{\Theta}(\xi)$ is an $M \times N$ variable random sensing matrix, whose elements are $\Theta[m, n] = \exp(j2\pi\xi[n]\delta_\upsilon T_m)$, the perturbation $\mathbf{w} = \mathbf{c} + \mathbf{n}$ represents clutter $\mathbf{c}$

plus noise $\mathbf{n}$, $\boldsymbol{\alpha}$ is the 'scene' vector with $\alpha_n = A_k$ if target k locates at $\xi[n]\delta_\upsilon$ and zero else, $n = 0, \ldots, N-1$, $\delta_\upsilon = 1/MT_r$ and

$$\xi[n] = \begin{cases} \upsilon_k/\delta_\upsilon, & \text{if } |\upsilon_k - n\delta_\upsilon| < \delta_\upsilon/2 \\ \upsilon_k/\delta_\upsilon, & \text{if } \upsilon_k - n\delta_\upsilon = \delta_\upsilon/2 \\ n & \text{else} \end{cases} \tag{4}$$

In this paper, we further assume that the clutter and noise are all Gaussian distributed and mutually independent. Clutter $\mathbf{c}$ is zero-mean with covariance matrix $\mathbf{R_c}$ and noise $\mathbf{n}$ is zero-mean with covariance matrix $\sigma^2\mathbf{I}_M$ ($\mathbf{I}_M$ is the identity matrix of size M).

If the signal-to-clutter ratio (SCR) and signal-to-noise ratio (SNR) are sufficiently high, the random matrix $\boldsymbol{\Theta}$ can be regarded to satisfy the RIP approximately. Unfortunately, the land clutter is always much stronger than the targets, which can violate the assumptions for CS severely [19]. The approaches of clutter cancellation by pre-processing [11] and weighting [14] are two practical ways to preserve the favorable properties of CS provided that the clutter spectrum is estimated as a prior knowledge. Therefore, the key requirement is the accurate estimation of clutter PSD.

2.2. Spectrum Estimation with CS-IGO

Traditionally, autoregressive model together with Burg's algorithm can obtain an effective estimation of the clutter by using sufficient i.i.d. training data [9]. However, it doesn't work well if the range stationarity is destroyed. So we propose a new approach similar to D3 in STAP [15–17] with only the test cell by exploiting the priori sparsity of the clutter spectrum.

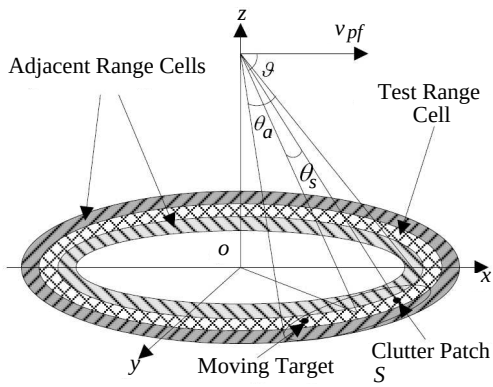

Figure 1. Geometry of airborne radar for moving target detection.

Assume there are only mainlobe clutters in the echo which are caused by stable objects like mountains and buildings [10]. As shown in Fig. 1, it is well known that the Doppler frequency component of mainlobe clutter is approximately limited within

$$\Delta\upsilon = [2v_{pf}\cos(\vartheta + \theta_a/2)/\lambda,\ 2v_{pf}\cos(\vartheta - \theta_a/2)/\lambda] \tag{5}$$

where v_{pf} is the platform velocity, λ the radar wavelength, θ_a azimuth beamwidth, and ϑ the angle between the velocity vector and the beam axis. In order to enlarge the non-clutter area in Doppler domain, the number of Doppler cells can be increased as large as the matrix RIP holds owe to the unambiguity, and also narrow beamwidth is always formed which leads to small number cells of clutter compared with the whole Doppler cells. Thus, the significant elements only exist in the area of the mainlobe as well as several discrete target positions, which guarantees sparsity of the spectrum.

Assume the clutter $\mathbf{c}$ in the test range cell can also be represented by S statistical independent scatter patches with complex amplitudes C_s and corresponding Doppler frequencies υ_s, that is

$$c[m] = \sum_{s=1}^{S} C_s \exp(j2\pi\upsilon_s T_m) \tag{6}$$

where $\upsilon_s = 2v_{pf}\cos(\vartheta + \theta_s)/\lambda \in \Delta\upsilon$ with θ_s as the corn angle between the beam axis and the look direction, then the clutter model can be represented as

$$\mathbf{c} = \boldsymbol{\Theta}_c(\xi_c)\boldsymbol{\alpha}_c \tag{7}$$

where $\boldsymbol{\Theta}_c(\boldsymbol{\xi}_c)$ and $\boldsymbol{\alpha}_c$ represent the sensing matrix and 'scene' vector of the clutter, which are similar to that of the targets. Finally, the signal model can be modified as

$$\mathbf{s}_r = \boldsymbol{\Theta}'(\xi')\boldsymbol{\alpha}' + \mathbf{n} \tag{8}$$

where $\boldsymbol{\Theta}'(\xi')$ and $\boldsymbol{\alpha}'$ correspond to the new Doppler 'grids' $\xi'[n]\delta_\upsilon$ and complex amplitudes containing both targets and clutter.

If only we knew the exact ξ', we could directly apply the l_1 minimization method to obtain the parameters by solving the following convex optimization problem

$$\hat{\boldsymbol{\alpha}}' = \arg\min_{\boldsymbol{\alpha}'} \left\|\boldsymbol{\alpha}'\right\|_1 \text{ subject to } \left\|\mathbf{s}_r - \boldsymbol{\Theta}'(\xi')\boldsymbol{\alpha}'\right\|_2 \le \varepsilon \tag{9}$$

where $\hat{\varepsilon} \approx \sqrt{M\hat{\sigma}^2}$ is the noise level determined by the noise variance $\hat{\sigma}^2$, which plays a significant role on the recovery performance of (9). For example, if it is set to be too small or too large, in the reconstruction, either a significant part of the strong noise is treated as signal or the acquired signal components are not fully reconstructed, resulting in

distortion due to too many false components or too few strong true components. In our situation, the noise level can be almost exactly estimated by using the nearby range cells with no clutter following the method proposed in [13].

In practice, however, we always have no priori information of the perfect Doppler 'grids', which may lead to unacceptable results with direct CS method suffering from serious mismatch effect. Therefore,

Table 1. The iterative grid optimization algorithm.

Input: The signal sampling vector $\mathbf{s}_r \in \mathbb{R}^M$, the random PRI T_m, the estimated noise bound ε, the error threshold Ξ, the maximum number of iterations $L_{\max}$, the Doppler resolution $\delta_v = 1/MT_r$, the number of Doppler cells $N > M$, initialization $\sigma_\xi^{(0)} = \sigma_n^{(0)} = 1$, $l = 0$, the elements of $\hat{\xi}'^{(loop)}$ are set as $\hat{\xi}'^{(loop)}[n] = n$, $loop = 0, \ldots, L_{\max} - 1$, $n = 0, \ldots, N-1$.
Output: The final sensing matrix $\boldsymbol{\Theta}'(\hat{\xi}')$ and the spectrum estimation $\hat{\alpha}'$ with clutters and targets.
Step1: Compute $\boldsymbol{\Theta}'^{(0)}$ from $\hat{\xi}'^{(0)}$ and obtain the coarse spectrum $\hat{\boldsymbol{\alpha}}'^{(0)}$ by using (9).
Step2: Set $l = l + 1$ and estimate the support set vector $\boldsymbol{\Lambda}^{(l)}$ of $\hat{\boldsymbol{\alpha}}'^{(l-1)}$ by constant false alarm rate (CFAR) detection to form $K^{(l)}$, $\hat{\boldsymbol{\alpha}}'^{(l)}_{\boldsymbol{\Lambda}}$ and $\boldsymbol{\Theta}^{(l)}_{\boldsymbol{\Lambda}}$, where $K^{(l)}$ is the vector length of $\boldsymbol{\Lambda}^{(l)}$, $\hat{\boldsymbol{\alpha}}'^{(l)}_{\boldsymbol{\Lambda}}$, $\boldsymbol{\Theta}^{(l)}_{\boldsymbol{\Lambda}}$ denote the elements and columns in $\hat{\boldsymbol{\alpha}}'^{(l-1)}$, $\boldsymbol{\Theta}'^{(0)}$ indexed within $\boldsymbol{\Lambda}^{(l)}$.
Step3: Compute $\hat{\mathbf{A}}^{(l)}_{\mathbf{a}}$ as well as $\hat{\mathbf{A}}^{+(l)}_{\mathbf{a}}$ by using $\boldsymbol{\Lambda}^{(l)}$, $\hat{\mathbf{a}}'^{(l)}_{\boldsymbol{\Lambda}}$, $\sigma_\xi^{(l-1)}$ and $\sigma_n^{(l-1)}$ according to $\mathbf{A}_{\mathbf{a}} = [\sigma_\xi \boldsymbol{\Phi}_\xi, \sigma_n \mathbf{I}_M]$, where $\mathbf{A}^+_{\mathbf{a}}$ is the pseudo-inverse of $\mathbf{A}_{\mathbf{a}}$, $\Phi_\beta[m,k] = j2\pi T_m \exp(j2\pi\Lambda[k]\delta_v T_m)a'_{\boldsymbol{\Lambda}}[k]$, $a'_{\boldsymbol{\Lambda}}[k]$ denotes the kth coefficient in $\hat{\mathbf{a}}'^{(l)}_{\boldsymbol{\Lambda}}$ and $k = 0, \ldots, K^{(l)} - 1$.
Step4: Update $\hat{\mathbf{a}}'^{(l)}_{\boldsymbol{\Lambda}}$ according to $\hat{\mathbf{a}}_{\boldsymbol{\Lambda}} = (\mathbf{H}^H\mathbf{H})^{-1}\mathbf{H}^H\mathbf{y}$ where $\mathbf{H} = \hat{\mathbf{A}}^{+(l)}_{\mathbf{a}}\boldsymbol{\Theta}^{(l)}_{\boldsymbol{\Lambda}}$ and $\mathbf{y} = \hat{\mathbf{A}}^{+(l)}_{\mathbf{a}}\mathbf{s}_r$.
Step5: Compute $\hat{\mathbf{e}}^{(l)}$ according to $\hat{\mathbf{e}}^{(l)} = \hat{\mathbf{A}}^{+(l)}_{\mathbf{a}}(\mathbf{s}_r - \boldsymbol{\Theta}^{(l)}_{\boldsymbol{\Lambda}}\hat{\mathbf{a}}^{(l)}_{\boldsymbol{\Lambda}})$ and $\left(\xi'^{(l)}\right)_{\boldsymbol{\Lambda}^{(l)}} = \left(\xi'^{(l-1)}\right)_{\boldsymbol{\Lambda}^{(l)}} + \frac{\sigma_\xi^{(l-1)}}{\delta_v}\mathrm{real}\left(\hat{e}^{(l)}[k]\right)\Big|_{k=1}^{K^{(l)}}$.
Step6: If $\left\|\xi'^{(l)} - \xi'^{(l-1)}\right\|_2 \le \Xi$ or $l = L_{\max}$, return $\boldsymbol{\Theta}'(\xi'^{(l)})$, $\hat{\boldsymbol{\alpha}}'^{(l-1)}$, stop; else reconstruct $\hat{\mathbf{a}}'^{(l)}$ with (9), compute $\sigma_\xi^{(l)} = \sqrt{\sum_{k=0}^{K^{(l)}-1}\left|\hat{e}^{(l)}[k]\right|^2}$, $\sigma_n^{(l)} = \sqrt{\sum_{k=K^{(l)}}^{K^{(l)}+M-1}\left|\hat{e}^{(l)}[k]\right|^2}$ and go to Step 2.

in our situation the CS-IGO algorithm is used by deeming the clutter as signals with high SNR. By updating the 'grids' with estimated mismatch error iteratively to achieve better signal model fit, the parameter estimation mean-squared error is close to the Cramer-Rao lower bound (CRLB). And then the final sensing matrix $\hat{\Theta}'(\hat{\xi}')$ and the spectrum estimation $\hat{\boldsymbol{\alpha}}'$ with clutters and targets can be well obtained, which is summarized in Table 1.

3. CLUTTER SUPPRESSION WITH PRE-FILTER AND REWEIGHTED L_1 MINIMIZATION

Because some of the target energy may be losing during the procedure of linear optimization, further adaptive processing for clutter suppression is necessary for subsequent target detection. Considering that the mainlobe clutter is localized and strong in the spectrum whose boundary can be determined by the prior knowledge, we improve the optimization problem from two different aspects: The first is to utilize a pre-filter to cancel the mainlobe clutter, and the second is to construct a reweighted optimization penalty to suppress the residue. As we deem all the components within the boundary as clutter, further assumption should be made that the spectrum of clutter does not overlap with that of targets' spectrum.

3.1. Suppression of Mainlobe Clutter with Pre-filter

In classical processing, cancellation for mainlobe clutter is often performed simply by designing a notch filter, which is mathematically represented as a projection to the clutter free subspace. The same procedure can be performed for the CS processing. Generally, the pre-filter can be represented by an $M \times M$ nonsingular matrix $\mathbf{F}$. The sensing matrix is modified to $\mathbf{F}\boldsymbol{\Theta}'$, and the filtered perturbation $\mathbf{Fw}$ contains only noise if the clutter contribution is totally removed. Then the target spectrum $\hat{\boldsymbol{\alpha}}_T$ can be obtained by solving the following transformed optimization problem:

$$\hat{\boldsymbol{\alpha}}_T = \arg\min_{\boldsymbol{\alpha}} \|\boldsymbol{\alpha}\|_1 \text{ subject to } \left\|\mathbf{F}\mathbf{s}_r - \mathbf{F}\hat{\boldsymbol{\Theta}}'(\hat{\xi}')\boldsymbol{\alpha}\right\|_2 \leq \eta \tag{10}$$

where $\eta = \|\mathbf{Fw}\|_2$ is the noise level after projection, which can also be estimated by the method proposed in [13] if $\mathbf{F}$ is obtained. As $\hat{\boldsymbol{\Theta}}'(\hat{\xi}')$ has already been obtained in (9), the only unknown part of (10) is the pre-filter matrix $\mathbf{F}$. Therefore, we will focus on the problem of how to form $\mathbf{F}$ as follows.

In our specific case of airborne systems, because the location of mainlobe clutter in the estimated Doppler spectrum $\hat{\boldsymbol{\alpha}}'$ is determined

by the platform velocity, the radar wavelength, the look direction and the beamwidth as in (5), all values of which are a prior knowledge when the radar works [20]. Therefore the boundary of clutter can be obtained approximately. Then the estimated clutter can be effectively obtained as

$$\hat{\mathbf{c}} = \hat{\boldsymbol{\Theta}}'(\hat{\boldsymbol{\xi}}')\boldsymbol{\Sigma}\hat{\boldsymbol{\alpha}}' \tag{11}$$

where $\boldsymbol{\Sigma}$ represents a diagonal matrix with elements ones corresponding to the locations with clutter on the diagonal and zeros else. Then the estimated CCM is given by

$$\hat{\mathbf{R}}_{\mathbf{c}} = \hat{\mathbf{c}}\hat{\mathbf{c}}^H = \hat{\boldsymbol{\Theta}}'(\hat{\xi}')\boldsymbol{\Sigma}\hat{\boldsymbol{\alpha}'}\hat{\boldsymbol{\alpha}'}^H\boldsymbol{\Sigma}^H(\hat{\boldsymbol{\Theta}}'(\hat{\boldsymbol{\xi}}'))^H \tag{12}$$

which is proved to be an positive semi-definite Hermite matrix where $(\cdot)^H$ denotes conjugate transpose.

Proof: The CCM is obviously an Hermite matrix by testifying $\hat{\mathbf{R}}_{\mathbf{c}}^H = (\hat{\mathbf{c}}\hat{\mathbf{c}}^H)^H = \hat{\mathbf{c}}\hat{\mathbf{c}}^H = \hat{\mathbf{R}}_{\mathbf{c}}$. In order to prove its property of positive semi-definite, we rewriter the CCM as the matrix form

$$\hat{\mathbf{R}}_{\mathbf{c}} = \begin{bmatrix} \hat{c}_0\hat{c}_0^* & \hat{c}_0\hat{c}_1^* & \cdots & \hat{c}_0\hat{c}_{M-1}^* \\ \hat{c}_1\hat{c}_0^* & \hat{c}_1\hat{c}_1^* & \cdots & \hat{c}_1\hat{c}_{M-1}^* \\ \vdots & \vdots & \ddots & \vdots \\ \hat{c}_{M-1}\hat{c}_0^* & \hat{c}_{M-1}\hat{c}_1^* & \cdots & \hat{c}_{M-1}\hat{c}_{M-1}^* \end{bmatrix} \tag{13}$$

where $\hat{c}_p$ denotes the pth element in $\hat{\mathbf{c}}$, and $(\cdot)^*$ denotes conjugate. For any given vector $\mathbf{z} = [z_0, \ldots, z_{M-1}]^T \in \mathrm{C}^{M\times 1}$, we have

$$\mathbf{z}^H\hat{\mathbf{R}}_{\mathbf{c}}\mathbf{z} = \sum_{p=0}^{M-1}\sum_{q=0}^{M-1} z_p^*\hat{c}_p\hat{c}_q^*z_q = \left(\sum_{p=0}^{M-1} z_p^*\hat{c}_p\right)\left(\sum_{q=0}^{M-1} z_q^*\hat{c}_q\right)^* = \left|\sum_{p=0}^{M-1} z_p^*\hat{c}_p\right|^2 \geq 0 \tag{14}$$

Therefore, the CCM is positive semi-definite according to the definition, thus proves $\hat{\mathbf{R}}_{\mathbf{c}}$ the positive semi-definite Hermite matrix.

Notate $\hat{\sigma}^2$ as the estimated noise variance and then the estimated covariance matrix of the perturbation $\mathbf{w}$ can be estimated as

$$\hat{\mathbf{R}}_{\mathbf{w}} = \hat{\mathbf{R}}_{\mathbf{c}} + \hat{\sigma}^2\mathbf{I}_M \tag{15}$$

which is obviously positive definite and can be expressed by Cholesky factorization $\hat{\mathbf{R}}_{\mathbf{w}} = \mathbf{D}^H\mathbf{D}$ with a nonsingular matrix $\mathbf{D}$. Finally the adaptive prewhitening filter can be derived as

$$\mathbf{F} = (\mathbf{D}^{-1})^H \tag{16}$$

In order to see the prewhitening effect, we can testify the covariance matrix of $\mathbf{w}' = \mathbf{F}\mathbf{w}$ as follows

$$\begin{aligned} \hat{\mathbf{R}}_{\mathbf{w}'} &= E(\mathbf{w}'\mathbf{w}'^H) = E(\mathbf{F}\mathbf{w}\mathbf{w}^H\mathbf{F}^H) = \mathbf{F}E(\mathbf{w}\mathbf{w}^H)\mathbf{F}^H \approx \mathbf{F}\hat{\mathbf{R}}_{\mathbf{w}}\mathbf{F}^H \\ &= \mathbf{F}\mathbf{D}^H\mathbf{D}\mathbf{F}^H = \mathbf{I}_M \end{aligned} \tag{17}$$

which leads to the noise level $\eta = \|\mathbf{F}\mathbf{w}\|_2 \approx \sqrt{M}$.

3.2. Further Suppression of Clutter Residue by Reweighted L_1 Minimization

By the pre-filter, the strong clutters are almost suppressed without doing harm to the reconstruction process. However, as the prewhitening filter is not perfect, we construct a weighted optimization penalty in (10) to suppress the residue. In terms of forming target spectrum with high quality, one usually needs extraction of the strongest signal components and rejection of others such as clutter/noise residue. Considering that the discrimination between targets and clutter/noise in the spectrum corresponds to their amplitude difference, we make a distinction in the penalty function. Instinctively, a weighted formulation of l_1 minimization can be designed as

$$\hat{\boldsymbol{\alpha}}'_T = \arg\min_{\boldsymbol{\alpha}} \|\mathbf{W}\boldsymbol{\alpha}\|_1 \text{ subject to } \left\|\mathbf{F}\mathbf{s}_r - F\hat{\boldsymbol{\Theta}}'(\hat{\boldsymbol{\xi}}')\boldsymbol{\alpha}\right\|_2 \leq \eta \qquad (18)$$

where $\mathbf{W}$ is the diagonal matrix with the corresponding weight w_i for the ith component of on the diagonal and zeros elsewhere. As illuminated in [14], small weights could be used to encourage the recovery of strong components, while the large weights used potentially suppress the small ones. In our special case, as the target spectrum $\hat{\boldsymbol{\alpha}}$ with small clutter residue has been obtained by (10), we consider to assign weights directly according to the spectrum. For example, the weight for the ith coefficient of $\boldsymbol{\alpha}$ can be calculated as

$$w_i = \begin{cases} \frac{1}{|\hat{\alpha}_T(i)|}, & |\hat{\alpha}_T(i)| \neq 0 \\ \frac{1}{\varsigma}, & |\hat{\alpha}_T(i)| = 0 \end{cases} \qquad (19)$$

where $\hat{\alpha}(i)$ denotes the ith component of $\hat{\boldsymbol{\alpha}}$. Because the spectrum $\hat{\boldsymbol{\alpha}}$ is recovered by l_1 minimization, it is always sparse with many zero elements. To ensures the existence of $\mathbf{W}^{-1}$, we introduce a small constant ς which can be preset as

$$\varsigma = \arg\min_{|\hat{\alpha}_T(i)|} \left\{ |\hat{\alpha}_T(i)||_{i=0}^{N-1}, |\hat{\alpha}_T(i)| \neq 0 \right\} \qquad (20)$$

Then, these weights can be applied in (21) to encourage the signal support and suppress the residual clutter support.

To solve the problem more efficiently, a modification of (18) is given by

$$\hat{\mathbf{x}} = \arg\min_{\mathbf{x}} \|\mathbf{x}\|_1 \text{ subject to } \left\|\mathbf{F}\mathbf{s}_r - \mathbf{F}\hat{\boldsymbol{\Theta}}'(\hat{\xi}')\mathbf{W}^{-1}\mathbf{x}\right\|_2 \leq \eta \qquad (21)$$

and we have $\hat{\boldsymbol{\alpha}'}_T = \mathbf{W}^{-1}\hat{\mathbf{x}}$. Herein, the weights are applied to the matrix but not to the coefficients to estimate. Thus, we can also directly use l_1 minimization method.

Table 2. The iterative reweighted L_1 minimization algorithm.

Input: The obtained signal $\mathbf{Fs}_r$ and sensing matrix $\mathbf{F}\hat{\mathbf{\Theta}}'(\hat{\xi}')$, the estimated noise bound η, the error threshold Ξ', the maximum number of iterations $L'_{\max}$, initialization $l'=0$, the estimated target spectrum with clutter residue $\hat{\boldsymbol{\alpha}}_T^{(0)}=\hat{\boldsymbol{\alpha}}_T$ obtained by (10), the weight matrix $\mathbf{W}^{(0)}$ calculated by (19) and (20). Output: The final estimated target spectrum $\hat{\boldsymbol{\alpha}}_{TF}$.

Step1: Solve the weighted l_1 minimization problem $\hat{\mathbf{x}}^{(l'+1)}=\arg\min_{\mathbf{x}}\|\mathbf{x}\|_1$ subject to $\left\|\mathbf{Fs}_r-\mathbf{F}\hat{\mathbf{\Theta}}'(\hat{\xi}')\left(\mathbf{W}^{(l')}\right)^{-1}\mathbf{x}\right\|_2\le\eta$ then we have $\hat{\boldsymbol{\alpha}}_T^{(l'+1)}=\left(\mathbf{W}^{(l')}\right)^{-1}\hat{\mathbf{x}}^{(l'+1)}$.

Step2: If $\left\|\hat{\boldsymbol{\alpha}}_T^{(l'+1)}-\hat{\boldsymbol{\alpha}}_T^{(l')}\right\|_2\le\Xi'$ or $l'=L'_{\max}$, return $\hat{\boldsymbol{\alpha}}_T^{(l'+1)}$, stop; else update the weights by using $\hat{\boldsymbol{\alpha}}_T^{(l'+1)}$ to form $\mathbf{W}^{(l'+1)}$ with $w_i^{(l'+1)}=\begin{cases}\frac{1}{\left|\hat{\alpha}_T^{(l'+1)}(i)\right|}, & \left|\hat{\alpha}_T^{(l'+1)}(i)\right|\neq 0\\ \frac{1}{\varsigma^{(l'+1)}}, & \left|\hat{\alpha}_T^{(l'+1)}(i)\right|=0\end{cases}$

$\varsigma^{(l'+1)}=\arg\min_{\left|\hat{\alpha}_T^{(l'+1)}(i)\right|}\left\{\left|\hat{\alpha}_T^{(l'+1)}(i)\right|\Big|_{i=0}^{N-1},\left|\hat{\alpha}_T^{(l'+1)}(i)\right|\neq 0\right\}$

set $l'=l'+1$ and go to Step 1.

Moreover, in order to achieve successively better estimation of the nonzero coefficient locations, an iterative reweighted l_1 minimization algorithm [14] is used to construct the weights, which is shown in Table 2.

4. COMPLEMENTARY ISSUES AND DISCUSSIONS

After a series of processing, the targets' velocities and amplitudes can be finally obtained with considerable accuracy. However, it should be noted that there are several issues to be further explained.

Firstly, as the number of statistical independent clutter scatters distributed within the boundary may be more than that of the clutter Doppler cells, what we recovered by CS-IGO is not the exact clutter characteristics but the main components of the coherent summation

of all the scatters. Fortunately, due to the nearly orthogonal columns of the sensing matrix, the mainlobe clutter can be well represented by the Doppler cells within the boundary because the signal can be approximated sufficiently by a linear combination of the neighboring grids [11], and more precisely with out optimized grids. Moreover, when we transform the clutter spectrum back into the time domain, most of the clutter components and energy can be reserved, which hardly affects the design of pre-filter.

Secondly, apart from the l_1 minimization there are two additional iteration techniques in our approach, whose convergence properties are still not characterized completely. Because the sensing matrix is only approximately known at any intermediate iteration and hence the traditional proof techniques do not apply. In principle, given access to a sufficient number of measurements and high SNR, we may expect similar convergence behavior for the two algorithms as conventional CS algorithm. Empirically, they can be shown to be stable to small amounts of noise in the sparse signal, which can be demonstrated with the help of various numerical experiments in Section 5.

Finally, the approach's computational complexity is another concerned issue. It can be seen that the primary runtime cost is incurred in solving CS-IGO and iterative reweighted l_1 minimization, which are both determined by the performance of solving a linear system and the iteration number respectively. The overall runtime of the approach is relatively larger than traditional methods, which requires further investigation on fast l_1 minimization. However, these fast methods are not covered in this paper and our attention is mainly focused on sound clutter suppression with only the test range cell.

5. NUMERICAL SIMULATIONS

In this section, we conduct some simulations to demonstrate the effectiveness and the feasibility of the proposed method. Assume that the radar works on X-band whose wavelength is 0.03 m, the coherent processing interval is 6.4 ms and the width of each pulse in the train is 2 µs. We transmit $M = 64$ pulses and consider $N = 128$ Doppler cells. What's more, there are some preconditions to be demonstrated.

1) For the random PRI signal, the pulses are transmitted at time deviations which are selected in the coherent processing interval with discrete uniform distribution.

2) In the following simulations the SNR, SCR or clutter-to-noise ratio (CNR) represents for the sampling echo signal after down-conversion and low-pass filtering, which is added by the complex white Gaussian noise.

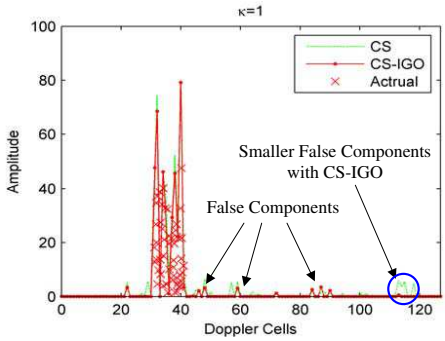

Figure 2. The estimated clutter spectrum with both direct CS and CS-IGO approaches under CNR = 10 dB.

3) For the clutter scenario, we directly assume that in the 31–40th Doppler cells there are 50 independent clutter scatters, each of which has a Gaussian distributed complex amplitude and a uniform distributed Doppler frequency.

4) All the convex optimization problems are solved by employing cvx [21] as an effective tool.

5) Our simulations are performed in MATLAB7 environment using a Pentium (R) 4 CPU 3.00 GHz processor with 1 GB of memory, and under Microsoft Windows XP operating system.

5.1. Clutter Spectrum Estimation by CS and CS-IGO

In this experiment, to characterize the clutter spectrum estimation performance of the proposed approach, we add white Gaussian noise to the echo signal with only clutter and no target, and both direct CS and CS-IGO approaches are used for clutter recovery.

Firstly, we perform several experimental trials under CNR = 10 dB and the typical estimated clutter spectrums with direct CS and CS-IGO approaches are shown in Fig. 2. It indicates that the 50 independent clutter scatters can be well represented by the 10 Doppler cells, which are regarded as main components of the coherent summation of all the scatters. What's more, the clutter spectrum with CS-IGO approach shows smaller false components than that of direct CS method, thus maintaining much more energy when we transform the clutter spectrum back into the time domain.

Secondly, in order to see the influence of estimated noise level to the convex optimization problem, we set $\varepsilon = \kappa\sqrt{M\sigma^2}$ with $\kappa = 1, 1.2, 1.4, 1.6$ respectively. Defining the clutter relative mean square

errors relative MSE (Relative MSE) as

$$\text{Relative MSE} = \|\hat{\mathbf{c}} - \mathbf{c}\|_2^2 / \|\mathbf{c}\|_2^2 \tag{22}$$

the distributions of relative MSEs under CNR=10 dB are shown in Fig. 3 with 100 Monte Carlo simulations. It can be seen from the histograms that the relative MSEs of clutters recovered by the CS-IGO approach are much smaller, which means more precise estimation. And we can observe another phenomenon that in both direct CS and CS-IGO, as the estimated noise level deviates form the true value, the estimation error of clutter increases obviously, which reflects the significance of exact estimation of noise level.

Thirdly, we will testify how noise influences the approach

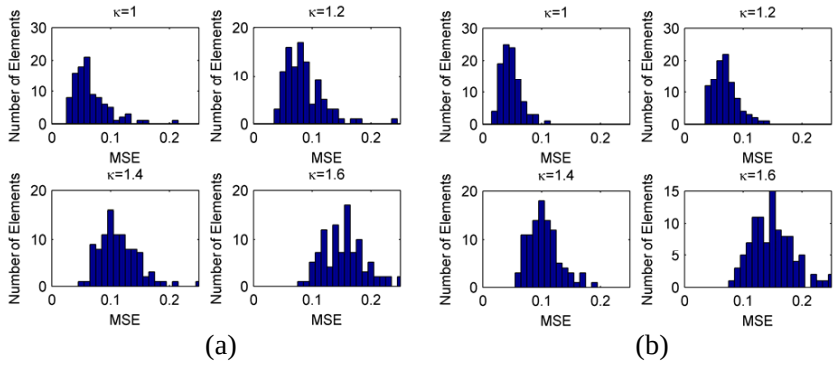

Figure 3. Distribution of clutter relative MSEs with different algorithms under CNR = 10 dB. (a) Direct CS. (b) CS-IGO.

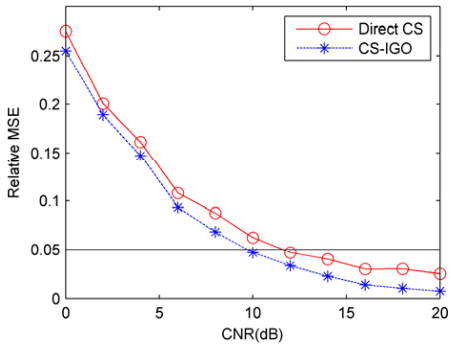

Figure 4. Relative MSEs of estimated clutter versus CNR with both direct CS and CS-IGO approaches.

performance. The relative MSE results of estimated clutters are calculated by averaging 50 Monte Carlo realizations under each CNR, which increases from 0 to 20 dB. As shown in Fig. 4, it is obvious that the performance meliorates with the increase of CNR. Especially, when CNR is above 10 dB the estimated clutter with CS-IGO changes slowly and the precision is always acceptable in practice, however, when CNR is below 10 dB the relative MSE increases sharply with the decrease of CNR, which is due to the sensitivity of CS theory to low CNR.

5.2. Comparison of Whitening Algorithms

In our first experiment, we will analyze the realization of weighting algorithm for whitening proposed in [9], the basic idea of which is to solve the following minimization problem

$$\hat{\boldsymbol{\alpha}}''_T = \arg\min_{\boldsymbol{\alpha}} \|\boldsymbol{\alpha}\|_1 \text{ subject to } \left\|\mathbf{s}_r - \hat{\boldsymbol{\Theta}}'(\hat{\xi}')(\hat{\boldsymbol{\alpha}}_{\mathbf{c}} \odot \boldsymbol{\alpha}/\zeta)\right\|_2 \leq \varepsilon \quad (23)$$

where $\hat{\boldsymbol{\alpha}}_{\mathbf{c}}$ is the estimated clutter spectrum, ζ a constant scale factor, and $\odot$ the Hadamard product. It is indicated in [9] that by the clutter whiten weighting clutter is suppressed to the noise level and $\hat{\boldsymbol{\alpha}}''_T$ only denotes the unambiguous Doppler spectrum of targets. In our particular situation, however, as the clutter spectrum $\hat{\boldsymbol{\alpha}}_{\mathbf{c}} = \boldsymbol{\Sigma}\hat{\boldsymbol{\alpha}}'$ is a sparse vector, those zero elements in the vector should be replaced with a small constant to guarantee the solvability of (23), and then the clutter spectrum for weighting can be represented as

$$\alpha_{\mathbf{c}}(i) = \begin{cases} |\alpha_{\mathbf{c}}(i)|, & \alpha_{\mathbf{c}}(i) \neq 0 \\ \zeta, & \alpha_{\mathbf{c}}(i) = 0 \end{cases} \quad (24)$$

where $\hat{\alpha}_{\mathbf{c}}(i)$ denotes the ith component of $\hat{\boldsymbol{\alpha}}_{\mathbf{c}}$. In practice, weighting is actually a sparse enhancement technique and weighting only the clutter supports is a locally sparse enhancement technique. Therefore, on the one hand, when the constant ζ is set too large, the clutter will not be so well whitened that large mainlobe clutter residue exists. On the other hand, when the constant ζ is set too small, the signal energy will weaken and even the joint optimization problem becomes irresolvable so that the target spectrum cannot be recovered.

Assume that there are three targets in the test range cell located randomly among the non-clutter Doppler area and SCR $= -10$ dB, SNR $= 10$ dB, we present the simulation results of a typical experiment. The original spectrum with CS-IGO and the target spectrums after weighting with $\zeta = 1, 10^{-2}, 10^{-4}$ are shown in Fig. 5 respectively. It can be seen that the weighting algorithm can well suppress the mainlobe clutter with proper value of constant ζ (e.g., $\zeta = 10^{-2}, 10^{-4}$) and the clutter residue will be decreased with the reduction of ζ. However, the

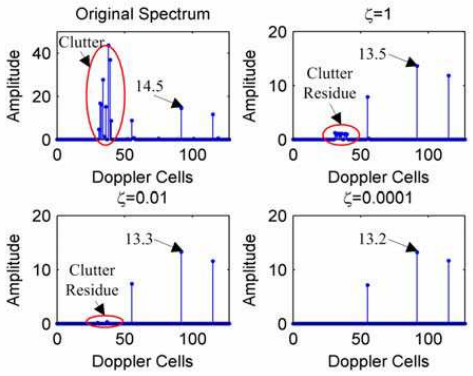

Figure 5. The original spectrum with CS-IGO and the target spectrums after weighting with different values of ζ.

signal energy will decrease simultaneously, and what's more, when the constant is set to $\zeta = 10^{-6}$, the optimization problem (23) becomes irresolvable and the target spectrum cannot be recovered. Therefore, it can be concluded that the value of ζ is crucial to the performance of weighting algorithm and it is hard to decide the value of ζ in a time varying clutter environment.

In the next experiment, we will compare the pre-filter whitening algorithm with the weighting algorithm. For justice, we consider the same scenario as in last subsection. By directly following the algorithm steps, the CCM and corresponding adaptive filter can be formed with the estimated clutter spectrum and noise variance. Then the target spectrum after pre-whitening is shown in Fig. 6(a), from which it can be seen that mainlobe clutter can also be well suppressed with our method. Further comparison to the spectrum by weighting algorithm (with $\zeta = 10^{-4}$) as shown in Fig. 6(b) indicates that, using our approach, the mainlobe clutter residue is more trivial and there are less energy losses of the targets. Most importantly, there is no parameter needed to be manually setting in our algorithm, which is more robust in practice. Although some sidelobe clutter residues appear in the spectrum, they can be suppressed by the iterative reweighted l_1 minimization algorithm, which is presented in Fig. 6(c). And finally the targets can be recovered with almost no clutter residue, which provides much high precision of amplitude and velocity estimation of the targets.

In order to compare the computational performance of the algorithms, we present the consumed time and memory cost in Table 3

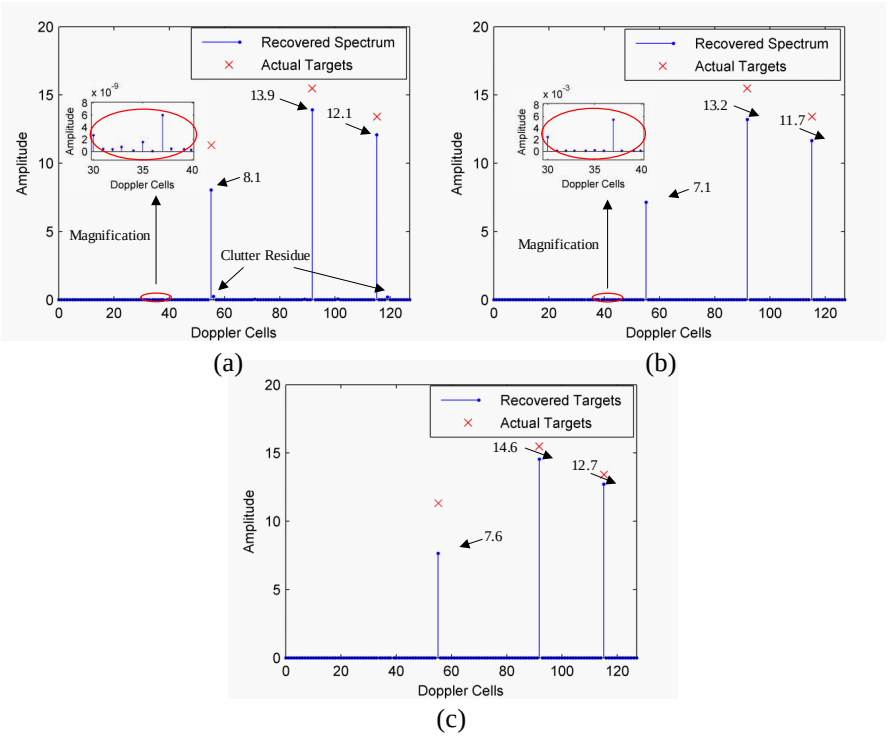

Figure 6. The recovered target spectrums with different whiten algorithms. (a) Pre-filtering. (b) Weighting with $\zeta = 10^{-4}$. (c) Pre-filtering and reweighted l_1 minimization.

Table 3. Performance and cost time of different algorithms.

Algorithms	Consumed Time (s)	Memory Cost (Double Complex)
Weighting	1.578	8384
Pre-filtering	1.659	12480
Pre-filtering and reweighted l_1 minimization	3.024	12480

for data size of $M = 64$ pulses and $N = 128$ Doppler cells. It can be seen from the table that pre-filtering is a litter more time-consuming and needs a larger memory cost than weighting due to calculation

and storage of the prefilter. For the pre-filtering and reweighted l_1 minimization method, as there are additional convex optimization problems, more time is consumed, however, the memory cost remains unchangeable. Although the cost time seems relatively much larger than traditional methods, some fast algorithms for the l_1-minimization problems have already been proposed [22–25], which is not covered in this paper.

5.3. Performance of Clutter Suppression

In order to characterize the clutter suppression performance of the proposed algorithm more quantitatively, the output SCNR defined in (25) and the normalized square errors (NSE) of the target amplitude modulus defined in (26) are calculated for a single target under each input SNR and SCR.

$$\text{SCNR} = 10\log_{10}\left[\left|\hat{A}\right|^2 / \left(\|\hat{\boldsymbol{\alpha}}_T\|_2^2 - \left|\hat{A}\right|^2\right)\right] \tag{25}$$

$$\text{NSE} = \left(\left|\hat{A}\right| - |A|\right)^2 / |A|^2 \tag{26}$$

where $\hat{A}$ is the estimated amplitude of the target, A the actual amplitude of the target, and $\hat{\boldsymbol{\alpha}}_T$ the recovered target spectrum. For comparison, the following four different clutter suppression schemes are used: a) weighting with $\zeta = 10^{-2}$; b) weighting with $\zeta = 10^{-4}$; c) pre-filtering; d) proposed algorithm by pre-filtering and reweighted l_1 minimization.

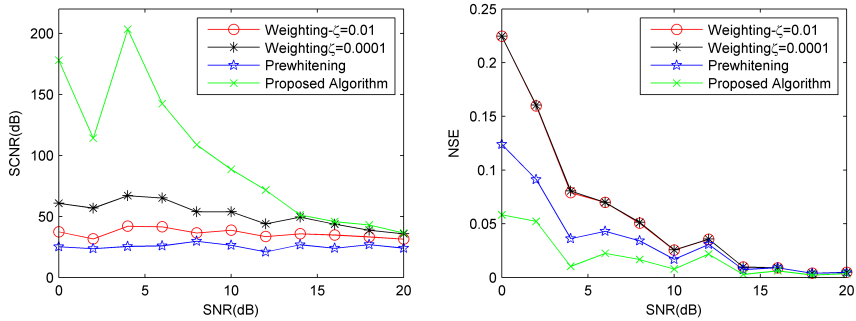

Figure 7. Performance of four different schemes under different SNRs. (a) Output SCNR versus SNR. (b) NSE versus SNR.

Firstly, by setting SCR $= -10$ dB, the output SCNR and NSE results are averaged over 50 independent Monte Carlo realizations under each SNR, which increases from 0 to 20 dB. It can be seen in Fig. 7 that, for the pre-filtering algorithm, although its output SCNR is a litter lower than the weighting algorithm, its amplitude precision is higher. Moreover, for the proposed algorithm by pre-filtering and reweighted l_1 minimization, its output SCNR and amplitude precision are both higher, which is more effective than merely weighting the clutter supports. Furthermore, as shown in Fig. 7(a), when the SNR is not very high, the targets can be recovered with almost no clutter residue by the proposed algorithm which leads to high output SCNR. However, when the SNR is higher than 14 dB, the output SCNR performance of the proposed algorithm is almost the same as that of weighting with $\zeta = 10^{-4}$. This is because that when the noise level is too low, the energy of sidelobe clutter residues after pre-filtering is comparable to the noise, which leads to small improvement of output SCNR by reweighted l_1 minimization and there is still some sidelobe clutter residues in the final spectrum.

Secondly, by setting SNR$=$ 10 dB, the output SCNR and NSE results are averaged over 50 independent Monte Carlo runs under each SCR, which decreases from 0 to -20 dB. As shown in Fig. 8, it can also be seen that under high SCRs (e.g. higher than -14 dB), the proposed clutter suppression scheme is much more effective than merely weighting the clutter supports. Similarly, it can be seen form Fig. 8(a) that when the SCR is lower than -14 dB, the output SCNR of the proposed algorithm is sometimes lower than that of the weighting algorithm, which is also caused by the large energy of sidelobe clutter residues after pre-filtering.

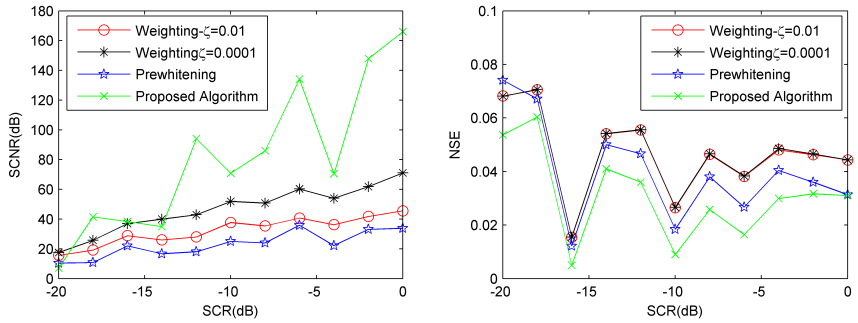

Figure 8. Performance of four different schemes under different SCRs. (a) Output SCNR versus SCR. (b) NSE versus SCR.

Finally, it can be concluded that the proposed algorithm performs well in amplitude estimation at all times and can improve the SCNR dramatically under proper situations, which is much more effective than merely weighting the clutter supports.

6. CONCLUSION

In this paper, an adaptive clutter suppression method is proposed for airborne random pulse repetition interval radar. After recovering the clutter spectrum with only the test range cell by exploiting its intrinsic sparsity, the optimization problem is improved by utilizing a pre-filter and an iterative weighted penalty, offering a high performance of amplitude precision and output SCNR in the nonhomogeneous clutter scenario. Simulation results demonstrate that the CS-IGO approach is more precise than direct CS method in estimating the clutter spectrum and the proposed clutter suppression scheme is also more effective than merely weighting the clutter supports. How to decrease the overall runtime of the approach and how to extend the approach to wideband imaging radar are underway.

ACKNOWLEDGMENT

This work is supported by the innovation project for excellent postgraduates of National University of Defense Technology under Grant B110404, and Hunan Provincial Innovation Foundation for Postgraduate under Grant CX2011B019. The authors would also like to thank the Editor and the anonymous reviewers for their helpful comments and suggestions to improve the quality of this paper.

REFERENCES

1. Kaveh, M. and G. R. Cooper, "Average ambiguity function for a randomly staggered pulse sequence," *IEEE Trans. Aerosp. Electron. Syst.*, Vol. 12, No. 3, 410–413, May 1976.
2. Vergara-Dominguez, L., "Analysis of the digital MTI filter with random PRI," *IEE Proceedings-F*, Vol. 140, No. 2, 129–137, Apr. 1993.
3. Cook, C. E. and M. Bernfeld, *Radar Signals: An Introduction to Theory and Application*, Academic Press, New York, 1967.
4. Donoho, D., "Compressed sensing," *IEEE Trans. Inf. Theory*, Vol. 52, No. 4, 1289–1306, Apr. 2006.

5. Candès, E. and T. Tao, "Near optimal signal recovery from random projections: Universal encoding strategies?" *IEEE Trans. Inf. Theory*, Vol. 52, No. 12, 5406–5425, Dec. 2006.
6. Candès, E., J. Romberg, and T. Tao, "Robust uncertainty principles: Exact signal reconstruction from highly incomplete frequency information," *IEEE Trans. Inf. Theory*, Vol. 52, No. 2, 489–509, Feb. 2006.
7. Wei, S. J., X. L. Zhang, J. Shi, and G. Xiang, "Sparse reconstruction for SAR imaging based on compressed sensing," *Progress In Electromagnetics Research*, Vol. 109, 63–81, 2010.
8. Wei, S. J., X. L. Zhang, and J. Shi, "Linear array SAR imaging via compressed sensing," *Progress In Electromagnetics Research*, Vol. 117, 299–319, Jun. 2011.
9. Quan, Y. H., L. Zhang, M. D. Xing, and Z. Bao, "Velocity ambiguity resolving for moving target indication by compressed sensing," *Electronics Letters*, Vol. 47, No. 22, Oct. 2011.
10. Barton, D. K. and S. A. Leonov, *Radar Technology Encyclopedia*, Artech House, Boston, London, 1998.
11. Ender, J. H. G., "On compressive sensing applied to radar," *Signal Processing*, No. 90, 1402–1414, 2010.
12. Khwaja, A. S. and J. Ma, "Applications of compressed sensing for SAR moving-target velocity estimation and image compression," *IEEE Transactions on Instrumentation and Measurement*, Vol. 60, No. 8, 2848–2860, 2011.
13. Zhang, L., M. Xing, C.-W. Qiu, J. Li, J. Sheng, Y. Li, et al., "Resolution enhancement for inversed synthetic aperture radar imaging under low SNR via improved compressive sensing," *IEEE Trans. Geosci. Remote Sens.*, Vol. 48, No. 10, 3824–3838, Oct. 2010.
14. Candès, E., M. Wakin, and S. Boyd, "Enhancing sparsity by reweighted l_1 minimization," *J. Fourier Anal. Appl.*, Vol. 14, No. 5, 877–905, Dec. 2008.
15. Sun, K., H. Meng, Y. Wang, and X. Wang, "Direct data domain STAP using sparse representation of clutter spectrum," *Signal Processing*, Vol. 91, No. 9, 2222–2236, 2011.
16. Choi, W., T. K. Sarkar, W. Hong, and E. L. Mokole, "Adaptive processing using real weights based on a direct data domain least squares approach," *IEEE Transactions on Antennas and Propagation*, Vol. 54, No. 1, 182–191, 2006.
17. Burintramart, S., T. K. Sarkar, Y. Zhang, and M. C. Wicks, "Performance comparison between statistical-based and direct

data domain STAPs," *Digital Signal Processing*, Vol. 17, 737–755, 2007.

18. Liu, Z., H. Wang, Y. Qin, and X. Li, "Adaptive clutter suppression for airborne random PRI radar based on improved compressed sensing," *Proc. CoSeRa2012*, 2012.
19. Levanon, N. and E. Mozeson, *Radar Signals*, Wiley, New York, 2004.
20. Zhang, M. and X. Wang, *Radar Systems*, Publishing House of Electronics Industry, Beijing, 2006.
21. Grant, M. and S. Boyd, "CVX: Matlab software for disciplined convex programming," http://stanford.edu/_boyd/cvxCVX, 2008.
22. Tropp, J. A. and S. J. Wright, "Computational methods for sparse solution of linear inverse problems," *Proceedings of the IEEE*, Vol. 98, No. 6, 948–958, Jun. 2010.
23. Yang, A. Y., A. Ganesh, Z. Zhou, S. S. Sastry, and Y. Ma, "A review of fast l_1-minimization algorithms for robust face recognition," http://arXiv:1007.3753v2 [cs.CV] 29 Jul 2010, 2010.
24. Mailhe, B., R. Gribonval, P. Vandergheynst, and F. Bimbot, "Fast orthogonal sparse approximation algorithms over local dictionaries," *Signal Processing*, doi:10.1016/j.sigpro.2011.01.004, 2011.
25. Donoho, D. L. and Y. Tsaig, "Fast solution of l_1-norm minimization problems when the solution may be sparse," *IEEE Trans. Inf. Theory*, Vol. 54, No. 11, 4789–4811, Nov. 2008.